




Cooperative Underwater Vehicle-Manipulator Operation Using Redundant Resolution Method

Jangho Bae¹ · Yecheol Moon² · Eugene Park³ · Jongwon Kim⁴ · Sangrok Jin⁵ · TaeWon Seo² 

Received: 11 October 2021 / Revised: 22 May 2022 / Accepted: 14 June 2022 / Published online: 26 July 2022

© The Author(s), under exclusive licence to Korean Society for Precision Engineering 2022, corrected publication 2022

Abstract

This paper presents a cooperative manipulation method for a dual-arm underwater vehicle-manipulator system (UVMS). The objective task is handle valve turning, which is a common underwater task. We propose a manipulation method that includes the concept of grasping a fixed structure such as a pipeline. While grasping a fixed structure and a handle valve, the entire system can be considered a parallel manipulator. Because of the kinematic properties of the system, the load for turning the handle valve can be distributed between the vehicle and the dual-arm manipulator, which means the vehicle can help with the operation of the manipulator. In addition, external disturbances such as oceanic currents can be efficiently compensated by using the proposed cooperative method due to the properties of the system. The kinematics and dynamics of the system were analyzed. The cooperative manipulation method was developed by modifying and adjusting redundancy resolution method with theory of a parallel manipulator. To prove the superiority of the method, a dual-arm UVMS was designed and fabricated. The advantages of the proposed cooperative method were validated through simulations and experiments.

Keywords Manipulators · Robot control · Unmanned underwater vehicles

1 Introduction

Underwater operations are very important for the progress of industries, however, underwater environments are hostile for human divers. An underwater vehicle-manipulator system (UVMS) can be a solution to this problem. Therefore, much research about UVMS focuses on intervention tasks, manipulating underwater components. The GIRONA500 autonomous underwater vehicle (AUV) was developed and conducted various intervention tasks by attaching a manipulator arm to the vehicle [1–4]. Khatib et al. developed a human-sized dual-arm UVMS, called Ocean One, and suggested possible tasks for application, such as inspection and intervention [5]. The valve intervention task is one important task performed in the underwater condition. Carrera et al. discussed the turning of underwater handle valves using an AUV with a manipulator by applying learning [6]. Youakim et al. conducted the underwater valve intervention task with a single arm manipulator attached on GIRONA500 AUV [7]. Di Lillo et al. succeeded to operate valves in oil rigs via satellite communication [8].

The common problem for designing mobile manipulator systems is power limitation of the system. Figure 1 shows the summarized data of commercial underwater manipulators

✉ Sangrok Jin
rokjin17@pusan.ac.kr

✉ TaeWon Seo
taewonsoo@hanyang.ac.kr

Jangho Bae
jangho.bae91@gmail.com

Yecheol Moon
mycm1302@hanyang.ac.kr

Eugene Park
eupark90@gmail.com

Jongwon Kim
jongkim@snu.ac.kr

¹ The School of Mechanical Engineering and Applied Mechanics, University of Pennsylvania, Philadelphia, PA 19104, USA

² The School of Mechanical Engineering, Hanyang University, Seoul 04763, Republic of Korea

³ Bluesink Robotics, Street, Seoul 08826, Republic of Korea

⁴ The Department of Mechanical Engineering, Seoul National University, Seoul 08826, Republic of Korea

⁵ The School of Mechanical Engineering, Pusan National University, Busan 46241, Republic of Korea

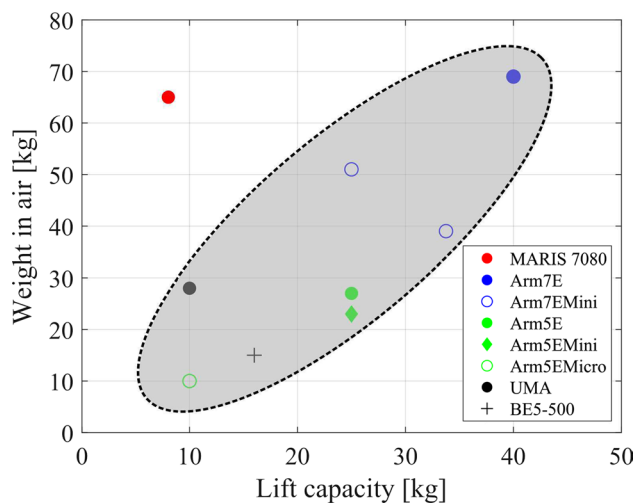


Fig. 1 Relation between weight in air and lift capacity of commercial underwater manipulators. Gray ellipsoid indicates the area that the most of commercial manipulators located, which shows the correlation between weight and capacity

based on a review of Sivčev et al. [9]. As shown in Fig. 1, the stronger the manipulator, the heavier it becomes. Therefore, the power of the manipulator is usually restricted by the size and performance of a mobile platform. To reduce this limitation, we propose the idea of cooperation between the manipulator and the vehicle to efficiently use the power of the whole system.

Cooperation between two subsystems, a mobile platform and a manipulator, can improve the overall performance of the entire system. Based on the cooperation between a mobile platform and a manipulator, the entire system can conduct the same task using a lighter manipulator. There have been many studies regarding the use of both the manipulator and mobile platform. Inoue et al. applied a whole-body control method for a wheeled mobile manipulator to withstand an external force [10]. Dietrich et al. used the whole-body control concept for compliance control of a Rollin' Justin robot [11]. Han et al. control both the manipulator and vehicle of a UVMS to minimize the restoration moment of the entire system [12]. Ryll et al. developed a novel hexacopter with tilted rotors and conducted various manipulation tasks with a fixed end-effector [13]. The proposed aerial vehicle can control all 6 DOFs and apply force and torque components independently. Therefore, the vehicle can conduct manipulation by using vehicle's thrust force. However, from the viewpoint of the cooperation concept, the distribution of task loads between two subsystems has yet to be studied.

We adopted the concept that the system grasps fixed an environmental structure during operation. In our previous study, we introduced the concept of grasping an underwater structure while performing a handle valve turning task [14],

and we proved the superiority this method through simulation [15]. From these results, we can assume that the system can be stabilized and is able to withstand large external disturbances. On an underwater system, stability is critical, as presented in Taylor's research [16]. This concept has typically been used on humanoid robots. Harada et al. improved the balancing performance of a humanoid robot by allowing it to grasp fixed environmental structures, such as handrails [17]. Koyanagi et al. developed an algorithm for generating the path of a humanoid robot on a rough surface and allowed it to use its arm to grasp a handrail [18]. The grasping concept has not only been used for humanoid robots but also for other types of robots. Lehmann et al. applied the grasping concept on a milling robot to improve its accuracy [19]. The grasping concept can significantly improve the performance of a UVMS. Khatib et al. addressed the possibility of using a fixed underwater structure for withstanding heavy currents [5]. Seki et al. applied this concept to a UVMS to increase the stability when maintaining the contact force of an end-effector [20].

A dual-arm manipulator was selected for developing our cooperative manipulation method. A single-arm is not sufficient for achieving the objectives of the research. A dual-arm manipulator can perform various tasks simultaneously because of its redundant DOF. Russakow et al. introduced an analysis and control method for a branch-shaped manipulator, and proved the validity of the method based on experimental results [21]. Casalino and Turetta suggested the singularity avoidance coordination for a non-holonomic mobile dual-arm manipulator system based on manipulability measurements [22]. Dietrich et al. summarized and compared previous redundancy resolution methods with their own proposed method through a simulation [23]. Korpela et al. attached a dual-arm manipulator to an aerial system and conducted a handle intervention experiment using a compliance controller [24]. Cataldi et al. introduced a layered kinematic controller for an aerial vehicle with a dual-arm manipulator and showed the advantages of the controller with experiments [25]. A dual-arm manipulator has also been used on various UVMSs, for example, Moe et al. applied a null space projection method to a planar dual-arm UVMS to achieve a main task and subtasks simultaneously [26].

In this study, a cooperative manipulation algorithm for a dual-arm UVMS was developed and verified with simulations and experiments. In our previous study, we developed an underwater vehicle tilting thruster underwater robot (TTURT) that can achieve motion with 6 degrees-of-freedom (DOF) using four tilting thrusters; this robot is shown in Fig. 2 [27]. The proposed underwater vehicle can be outfitted with various modules for specific tasks, such as the example shown in Fig. 2. We designed the dual-arm UVMS by attaching manipulator arm modules to our vehicle, TTURT. The turning of an underwater handle valve was

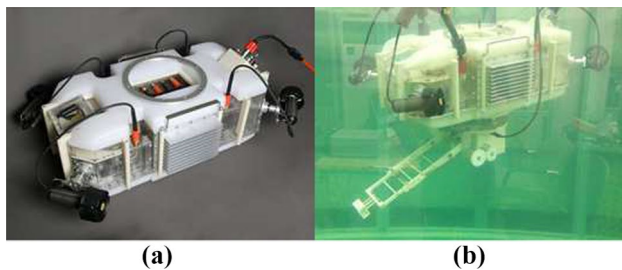


Fig. 2 Underwater vehicle TTURT: **a** appearance of the vehicle; **b** TTURT with single-arm manipulator module

selected as the objective task of the system because it is a demanding task that is in a challenging environment.

The contributions of this study are as follows. Kinematic modeling of the system for grasping both a fixed structure and a handle valve, which can be considered as a parallel manipulation, was developed and analyzed. By utilizing the kinematic properties of a closed-loop manipulator, a cooperative manipulation method that reduces the torque of the manipulator using the thrust force of the vehicle was developed. In addition, to cope with external disturbances during an operation, a disturbance compensation term was applied, which also includes a cooperation concept. The concept of cooperative manipulation is summarized by Fig. 3. This method was proved experimentally through the fabricating of a dual-arm UVMS and by conducting a valve turning operation on a test bed in a water tank.

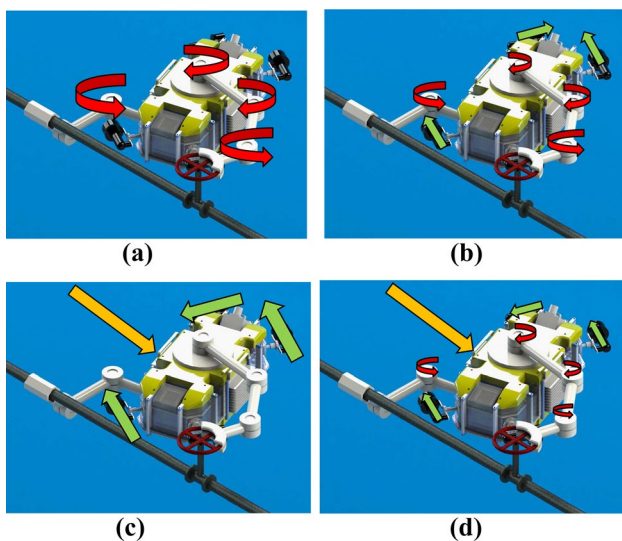


Fig. 3 The concept of the proposed cooperation manipulation method: **a** Non-cooperative valve turning operation; **b** Turning the handle valve with the aid of the vehicle thrust force; **c** Compensating disturbance with the vehicle only; **d** Compensating disturbance by cooperation with the vehicle and the manipulator

The remainder of this paper is organized as follows. In Section 2, the kinematics and dynamics of the system are modeled. Section 3 describes the cooperative manipulation algorithm applied between two subsystems. The cooperation manipulation results of simulations and experiments are given in Section 4. The experimental results under disturbance are presented and discussed in Section 5. Finally, concluding remarks are provided in Section 6.

2 System Modeling

2.1 Kinematics Modeling

As addressed in the Introduction, the dual-arm UVMS was designed by attaching two manipulator arm modules to the connecting point of our vehicle, TTURT. Because of the positions of the module connectors, one arm is attached to the top of the vehicle, and the other arm is attached to the bottom of the vehicle.

While grasping the pipeline, the entire system can be considered a parallel manipulator. Figure 4 shows a kinematics diagram of the system for grasping a pipe and a handle valve. The notations used for describing the UVMS are as follows. The upper arm, called a working manipulator, grabs the handle valve, and the lower arm, called a clamping manipulator, clamps the entire system to the fixed pipeline through a grasping action. The Earth-fixed frame of the system is denoted as $\{O\}$. The origin of the Earth-fixed frame is located at the grasping point of the clamping manipulator. The body-fixed frame is denoted as $\{B\}$, whereas the position of the end-effector frame of the working manipulator is denoted as $\{E\}$. The i -th joint of the working manipulator is represented as W_i in Fig. 4, the joint angle of which is denoted as q_{wi} . The length of the i -th linkage is represented

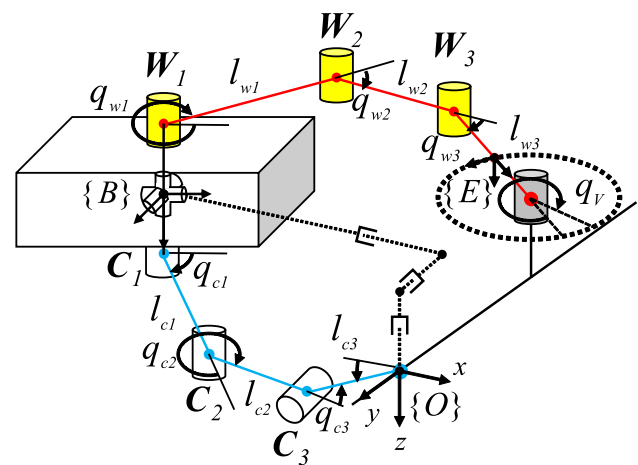


Fig. 4 Kinematics diagram with notations of the dual-arm UVMS

as l_{wi} . Similarly, for the i -th component of the clamping manipulator, the joint is denoted as C_i , the angle of which is represented as q_{ci} , and the length of the linkage is expressed as l_{ci} . The handle valve can be considered a virtual passive rotational joint, which is indicated by the gray colored joint in Fig. 4. The angle of this passive joint is represented as q_v . The position and orientation of the vehicle on an Earth-fixed frame can be assumed as a virtual 6-DOF joint [21]. The virtual 6-DOF joints are denoted as $\eta = [x \ y \ z \ \phi \ \theta \ \psi]^T$, where x, y, z are position and ϕ, θ, ψ are roll, pitch, yaw of the vehicle.

The kinematics of the UVMS were analyzed by following the theory of a parallel manipulator [28]. The system has three DOFs on the working plane [15]. To formulate the kinematic equation of the system, independent joints (q_u), which determine the configuration of the system, should be selected. The system has three DOFs, thus three joints of the working manipulator were selected as independent joints, which are denoted in yellow in Fig. 4; the other joints were categorized as dependent joints (q_v). Active joints are joints that are controlled by actuators. The rest of active joints except the independent joints are considered as the redundant joints. In this case, the virtual vehicle joints are those with respect to the Earth-fixed frame ($\eta = [x \ y \ z \ \phi \ \theta \ \psi]^T$), joints of the working manipulator ($q_w = [q_{w1} \ q_{w2} \ q_{w3}]^T$), and joints of the clamping manipulator ($q_c = [q_{c1} \ q_{c2} \ q_{c3}]^T$). The categorization of the joints is summarized in Table 1. The system is overactuated because the number of actuated joints is larger than the number of the independent joints.

A constraint Jacobian of the system must be derived to formulate the forward kinematics. The vehicle position derived from the joint angle and link lengths of working manipulator should be same as that derived from the clamping manipulator. The constraint equation of the system can be written as follows:

$$g(q_{all}) = [(\eta_w - \eta)^T, (\eta_c^* - [x, y, z, \psi]^T)^T]^T. \quad (1)$$

The vector η_w is the vehicle position and orientation derived from the working manipulator terms (q_w, l_{wi}). The vector η_c^* contains the position and yaw angle derived from the clamping manipulator terms (q_c, l_{ci}). The roll and pitch angles were removed because they were already constrained through the other constraints. The constraint equation vector (1) should be equal to zero.

Table 1 Joint classification of the UVMS

	Independent joints (q_u)	Active joints (q_r)	All joints (q_{all})
Joint vectors	$[q_{w1} \ q_{w2} \ q_{w3}]^T$	$[\eta^T \ q_w^T \ q_c^T]^T$	$[\eta^T \ q_w^T \ q_c^T \ q_v]^T$

The constraint Jacobian can be obtained by differentiating the constraint equations (1) as follows:

$$\frac{dg(q_{all})}{dt} = G\dot{q}_{all} = [G_u \ G_v] \begin{bmatrix} \dot{q}_u \\ \dot{q}_v \end{bmatrix} = 0, \quad (2)$$

where G_u and G_v are derived by rearranging columns of G . Equation (2) can be transformed as follow:

$$\dot{q}_{all} = \Lambda \dot{q}_u, \quad \dot{q}_r = \Gamma \dot{q}_u, \quad (3)$$

where the terms Λ and Γ are constraint Jacobians for the system.

The forward kinematics of the system can be derived by finding the relation between the velocity of the handle valve angle and independent joints. The handle valve angle is defined as an objective joint. The forward Jacobian was derived as follows:

$$\dot{q}_v = J\dot{q}_{all} = J_f \dot{q}_u. \quad (4)$$

The term J in (4) is the Jacobian between the valve angle and all joints, which can be directly derived. By using the relations in (2), the forward Jacobian J_f can be derived as (4). J_f is 1×3 matrix, because the system has kinematic redundancy.

2.2 Dynamics Modeling

The dynamic equation of the system was derived by applying the constraints of the system to a free-floating dynamic equation. The diagram of a free-floating dual-arm UVMS is shown in Figure 5. The dynamics of a free-floating UVMS can be derived by combining the methods of Spong [29] and Schjølberg [30]. The dynamics equation of the UVMS can thus be written as follows:

$$M(q_r, \dot{q}_r, \zeta)\ddot{\zeta} + D(q_r, \dot{q}_r, \zeta)\dot{\zeta} = \tau_r, \quad (5)$$

where ζ is body fixed velocity of the UVMS. The term M and D are defined as follows:

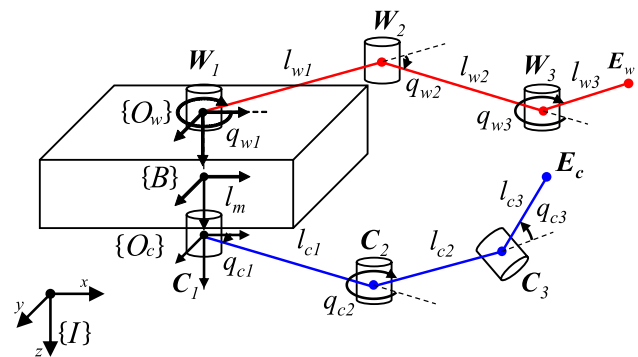


Fig. 5 Kinematics diagram with notations of the dual-arm UVMS

$$\mathbf{M}(q_r, \dot{q}_r, \zeta) = \begin{bmatrix} \mathbf{M}_{ve} + \mathbf{H}_w + \mathbf{H}_c & \mathbf{M}_{Cw} & \mathbf{M}_{Cc} \\ \mathbf{M}_{Cw}^T & \mathbf{M}_w & \mathbf{O} \\ \mathbf{M}_{Cc}^T & \mathbf{O} & \mathbf{M}_c \end{bmatrix}, \quad (6)$$

$$\mathbf{D}(q_r, \dot{q}_r, \zeta) = \begin{bmatrix} \mathbf{D}_{ve} + \mathbf{D}_{w1} + \mathbf{D}_{c1} & \mathbf{D}_{w2} & \mathbf{D}_{c2} \\ \mathbf{D}_{w3} & \mathbf{D}_{w4} & \mathbf{O} \\ \mathbf{D}_{c3} & \mathbf{O} & \mathbf{D}_{c4} \end{bmatrix}. \quad (7)$$

The terms \mathbf{M} and \mathbf{D} denote the total inertia and drag terms of the system. The terms \mathbf{M}_{ve} and \mathbf{D}_{ve} are the inertia and drag matrix of the vehicle, TTURT, which were derived in a previous study [27]. The other terms denoted with subscript w are related to the working manipulator and those denoted with subscript c are related to the clamping manipulator. In (6), the \mathbf{M}_* term is the inertia matrix of each manipulator, and the \mathbf{H}_* term is the additional vehicle inertia from the manipulators. The \mathbf{M}_{C*} term is the reaction between the vehicle and manipulators. In (7), \mathbf{D}_{*i} is the drag matrix of each manipulator itself, calculated by combining drag terms of each linkage. The other numbered term \mathbf{D}_{*i} is drag term generated by interactions between the vehicle and the manipulators.

By applying Cheng's method [31], the dynamics equation of a free-floating UVMS can be changed into the constrained dynamics of the proposed system. The inertia and drag matrix with respect to independent joint angles can be changed from the free-floating dynamics as follows:

$$\hat{\mathbf{M}} = \mathbf{A}^T \mathbf{M} \mathbf{A}, \quad (8)$$

$$\hat{\mathbf{D}} = \mathbf{A}^T \mathbf{M} \dot{\mathbf{A}} + \mathbf{A}^T \mathbf{D} \mathbf{A}, \quad (9)$$

where \mathbf{A} is the constraint Jacobian derived on (3). The constrained dynamics with respect to the independent joint angles can be derived as follows:

$$\hat{\mathbf{M}} \ddot{q}_u + \hat{\mathbf{D}} \dot{q}_u = \mathbf{F}^T \tau_r. \quad (10)$$

The term $\tau_r = [\tau_{ve}^T \ \tau_w^T \ \tau_c^T]^T$ indicates the force and torque of the actuated joints, q_r , which is a combination of the vehicle thrust force and torque, the torque of the working manipulator joints, and the torque of the clamping manipulator joints.

3 Cooperative Manipulation Algorithm

The proposed cooperative manipulation algorithm makes it possible to reduce the burden of the vehicle and the manipulator by grasping a stationary structure. Using the proposed algorithm, the required manipulator torque and vehicle thrust force were reduced, particularly under external disturbances [15]. As stated in the Introduction, we use a valve turning task as an example of applying the algorithm.

3.1 Desired Trajectory Generation

The objective of the UVMS is to turn an underwater handle valve, so a desired trajectory of the system should be generated. The shape and dimensions of the objective handle valve are shown in Fig. 6. The dimensions were set by referring to a standard handle valve with a diameter of 125 mm. As the desired end-effector trajectory, shown with the red arrows in Fig. 6, the handle valve is turned in the counter-clockwise direction at 90° starting from the 45° position. The angular speed of the valve was set as indicated in Fig. 6 c. The maximum value of the angular speed was set as $\frac{\pi}{48}$ (rad), and a second-order trajectory was used to prevent a sudden change in acceleration.

The desired trajectories of the independent joints were derived from the desired trajectory of the handle valve. The trajectories of the independent joints were generated to minimize the velocity vector norms of all actuated joints, $\|\dot{q}_r\|^2$. The term can be transformed as follows:

$$\|\dot{q}_r\|^2 = \dot{q}_u^T \mathbf{F}^T \mathbf{F} \dot{q}_u. \quad (11)$$

Although the system has three independent joints, there is one joint for describing the task space, the angle of the handle valve. Therefore, the system has kinematic redundancy on the task space. By modifying the Moore–Penrose pseudoinverse, the velocity vector norm of all actuated joints can be minimized as follows:

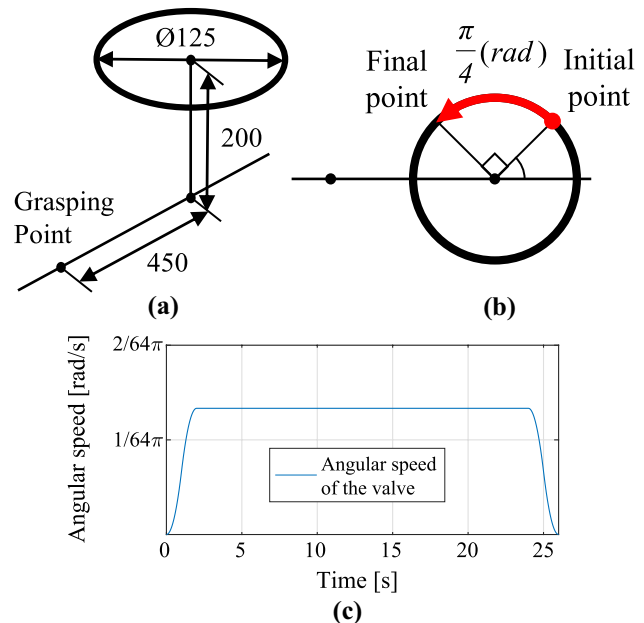


Fig. 6 Desired trajectory of end-effector: **a** shape and dimensions of the objective handle valve (all units are mm), **b** desired valve angle trajectory, and **c** desired angular speed of the valve

$$\dot{\mathbf{q}}_{u,d} = \mathbf{J}_f^\dagger \dot{\mathbf{q}}_{V,d}, \quad (12)$$

where

$$\mathbf{J}_f^\dagger = (\mathbf{J}_f^\top \mathbf{J}_f)^{-1} (\mathbf{J}_f^\top \mathbf{J}_f)^{-1}^\dagger. \quad (13)$$

Superscript (\dagger) denotes the Moore–Penrose pseudoinverse. The term $\dot{\mathbf{q}}_{V,d}$ denotes the desired angular velocity of the valve presented in Figure 6, and $\dot{\mathbf{q}}_{u,d}$ is the desired trajectory of the independent joints. The physical meaning of (12) is the same as minimizing the velocity vector norm of all actuated joints.

3.2 Cooperation in Main Task

Because of the kinematic properties of the system, the load for conducting a valve turning operation can be distributed between two subsystems, which means one subsystem can help the tasks of another subsystem. The system not only has kinematic redundancy, but also actuator redundancy. The controller for the system was developed by modifying the controller presented by Cheng [31]. The proportional-differential (PD) controller in the work space of the redundant parallel manipulator system can be derived as follows:

$$\boldsymbol{\tau}_{r,d} = (\mathbf{J}_f^\top)^\# (\mathbf{K}_D \dot{\mathbf{e}} + \mathbf{K}_P \mathbf{e}). \quad (14)$$

The matrix \mathbf{K}_P is the proportional gain of the controller, and the matrix \mathbf{K}_D is the differential gain. The vector $\boldsymbol{\tau}_{r,d}$ is the desired force and torque for the actuated joints used to follow the desired independent joint trajectory. The error term of independent joints \mathbf{e} is defined as follows:

$$\mathbf{e} = \mathbf{q}_{u,d} - \mathbf{q}_u. \quad (15)$$

In general, the Moore–Penrose pseudoinverse has been used for selecting the actuation force from a system that has actuator redundancy. In this case, a weighted pseudoinverse was used. The weighted pseudoinverse was denoted as superscript ($\#$) in (14), the definition of which is

$$(\mathbf{J}_f^\top)^\# = \mathbf{W}^{-1} (\mathbf{J}_f^\top \mathbf{W}^{-1})^\top, \quad (16)$$

and the physical meaning of which is minimizing $\boldsymbol{\tau}_r^\top \mathbf{W} \boldsymbol{\tau}_r$.

The weighting matrix for the proposed controller can be divided into components corresponding to each actuated

joint. The following equations show the weighting matrix of the cooperation method.

$$\mathbf{W} = \begin{bmatrix} \mathbf{W}_v & \mathbf{O} & \mathbf{O} \\ \mathbf{O} & \mathbf{W}_w & \mathbf{O} \\ \mathbf{O} & \mathbf{O} & \mathbf{W}_c \end{bmatrix}, \quad (17)$$

where

$$\mathbf{W}_v = \text{diag}(w_x, w_y, w_z, w_\phi, w_\theta, w_\psi), \quad (18)$$

$$\mathbf{W}_w = \text{diag}(w_{w1}, w_{w2}, w_{w3}), \quad (19)$$

$$\mathbf{W}_c = \text{diag}(w_{c1}, w_{c2}, w_{c3}). \quad (20)$$

Based on the physical meaning of weighted pseudoinverse, an active joint that has a high weighting will be minimized more. The diagonal components of the weighting matrix were set proportional to the reciprocal of the maximum possible force and the torque of the actuated joints and thrust components. Through this determination method, weak active joints apply less force or torque than stronger ones to conduct an objective task. Table 2 shows the maximum capacity of each active joint and diagonal components of the weighting matrix. The term $\tau_{mani,m}$ indicates a maximum torque of a manipulator joint, and w_{mani} denotes the weighting value of every manipulator joint. The components of the weighting matrix were normalized with respect to the reciprocal of the maximum capacity of the vehicle in the x -direction. Using this method, the task load is distributed between the vehicle and manipulators. The torque of the manipulator joints is minimized more than the vehicle thrust components because the strength of a manipulator joint is weaker than the vehicle thrust force.

The stability of the proposed method can be proved by following process.

$$\dot{V} = \frac{1}{2} \dot{\mathbf{q}}_u^\top \hat{\mathbf{M}} \dot{\mathbf{q}}_u + \frac{1}{2} \mathbf{q}_u^\top \mathbf{K}_P \mathbf{q}_u \quad (21)$$

$$\dot{V} = -\dot{\mathbf{q}}_u^\top (\mathbf{K}_v + 2\hat{\mathbf{D}}) \dot{\mathbf{q}}_u \quad (22)$$

$$\dot{V} \leq -\lambda_{\min}(\mathbf{K}_v + 2\hat{\mathbf{D}}) \|\dot{\mathbf{q}}_u\|^2 \quad (23)$$

Table 2 Values of maximum capacity of each joint and diagonal components of weighting matrix

$\tau_{x,m}$	$\tau_{y,m}$	$\tau_{z,m}$	$\tau_{\phi,m}$	$\tau_{\theta,m}$	$\tau_{\psi,m}$	$\tau_{mani,m}$
80 N	80 N	114 N	19 Nm	43 Nm	61 Nm	10 Nm
w_x	w_y	w_z	w_ϕ	w_θ	w_ψ	w_{mani}
1.00	1.00	0.71	4.35	1.88	1.33	8.09

By setting Lyapunov function V as (21), the time derivative of V was derived as (22). As derived in the above equations, if we set \mathbf{K}_v big enough, the controller is stable.

3.3 Cooperation in Compensating Disturbance

During operation, disturbances may be applied to the system, particularly to the vehicle. Due to the size of the vehicle, the vehicle takes most of the disturbance from the oceanic current. In our previous study, the external disturbance on the vehicle was efficiently compensated using a relatively small torque of the dual-arm manipulator while grabbing a handle valve [32]. Modifying and applying the disturbance compensating term to the proposed cooperative controller, the controller equation can be written as follows:

$$\tau_r = (\mathbf{\Gamma}^T)^\# (\mathbf{K}_D \dot{e} + \mathbf{K}_P e) + \tau_{dis}, \quad (24)$$

where

$$\tau_{dis} = (\mathbf{\Gamma}^T)^\# \mathbf{J}_b^T (-\mathbf{f}_d). \quad (25)$$

The vector τ_{dis} is the desired torque for compensating disturbance \mathbf{f}_d , which denotes the applied disturbance force applied to the vehicle. In this study, we assume that the disturbance force is accurately observed. The Jacobian matrix \mathbf{J}_b indicates the relation between the independent joint angles and the position and orientation of the vehicle.

Similar to the cooperation method of the main task, the cooperation concept can be applied to compensating a disturbance. In our previous study, the null space solution of Moore–Penrose pseudoinverse was used for deriving the compensating term. Instead, the weighted pseudoinverse was applied, as presented in (25). Using this method, the load for compensating the disturbance can also be distributed between two subsystems. The weighting matrix was set as the same matrix described in (17) and shown in Table 2.

Figure 7 shows the entire proposed cooperative controller of the UVMS. The desired velocities of independent joints $\dot{\mathbf{q}}_{u,d}$ are derived by trajectory generation presented on the previous section. The desired trajectories $\mathbf{q}_{u,d}$ were calculated by integrating $\dot{\mathbf{q}}_{u,d}$. The desired force and torque for valve turning were derived with the proposed cooperative

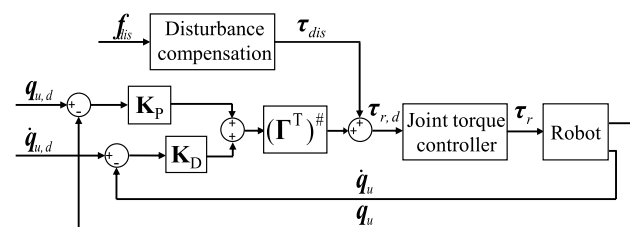


Fig. 7 The cooperative controller of the UVMS

method and the additional force and torque for compensating disturbance τ_{dis} were calculated as (25). These two terms are added together to get the desired force and torque $\tau_{r,d}$. The joint torque controller was added to make the joints of the dual-arm manipulator generate the desired torque from the controller. The joint torque controller will be presented in the following section.

4 Experimental Results of Cooperation

4.1 Simulation and Experiment Setups

The proposed cooperative manipulation method was proved through a dynamic simulation and experimental results. The simulation was developed using MATLAB/Simulink based on the dynamics equation (10). The proposed cooperative controller (14) was applied to the dynamics simulation and the performance of the cooperative controller was analyzed. The results of the simulations are discussed in the following section.

The dual-arm UVMS was fabricated to prove the advantages of the cooperative controller experimentally. To fabricate the underwater dual-arm manipulator, a joint module was designed. The detailed design of the joint module is shown in Fig. 8. A BLDC servo motor (ECflat60 100W, Maxon, Switzerland) and a Harmonic drive reducer (SCSD-17-100-2UF) were used in the actuator of the module. A torque transducer (SETech, Korea) was attached to the actuator assembly to measure the actual torque applied to the output axis. O-rings (Woosung Mectron, Korea) were located between the covers and main body, and a rotary seal (Woosung Mectron, Korea) was installed around the output axis to prevent flooding through the axis. High-density polyurethane foam is used as a buoyancy material to make the overall system neutrally buoyant. The foam is cut to fit the manipulator and attached around it.

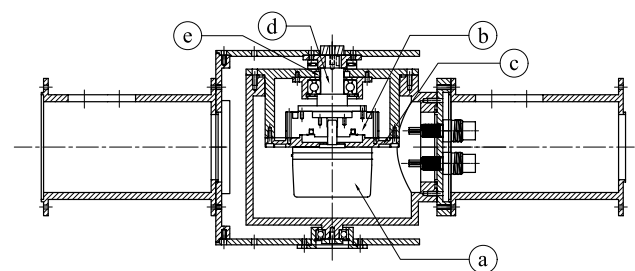


Fig. 8 Detailed drawing of the underwater joint module for the manipulator: **a** a BLDC servo motor (ECflat60 100W, Maxon, Switzerland); **b** a Harmonic drive reducer (SCSD-17-100-2UF, SBB, Korea); **c** a torque transducer (SETech, Korea); **d** a output axis; **e** a rotary seal (Woosung Mectron, Korea)

The joint torque controller was designed to make the joint module follow the desired torque from the proposed cooperative controller, as mentioned on Fig. 7. The proportional-integral (PI) controller was used to control the output torque. A process variable is set as the value of a torque sensor, and the control input is the motor driver duty value (command value of -4096 to 4096). Because of the rotary seal installed around the output axis, a high friction is applied to the output axis. This friction should be compensated to match the torque sensor value to apply torque to the output axis. Dahl's friction model [33] was used to estimate the friction of the rotary seal. Coefficients of the model were set using a movement experiment for each joint module. The joint module torque controller including the friction compensator is presented in Fig. 9.

The dual-arm manipulator for a UVMS was fabricated by connecting six joint modules with a pipe-shaped linkage. The link lengths of the UVMS were optimized as shown in Table 3, which were derived based on the results of our previous research [14]. Pneumatic air clamps were used as end-effectors of the dual-arm manipulator. The underwater valve structure was constructed using a standard handle valve in a water tank. Figure 10 shows the dual-arm UVMS turning a handle valve and grasping a pipe structure.

4.2 Valve Turning Experimental Results

The handle-valve turning experiments were conducted using a fabricated dual-arm UVMS, and two cases were compared. The first is the turning of a handle valve using only two manipulators, without vehicle thrust force, as in conventional systems. The second case is the turning of a handle valve using the proposed cooperative manipulation method. All experiments were conducted five times for each case, and the average data of the five experiments were applied to analyze the results. The torque of the C3 joint was neglected because this joint simply maintains the stationary position and is only influenced by a buoyancy error of the system.

Figure 11 shows the joint and vehicle trajectory of the dual-arm UVMS, while Fig. 12 shows the snapshots of the experiment video. The joint trajectories were measured from

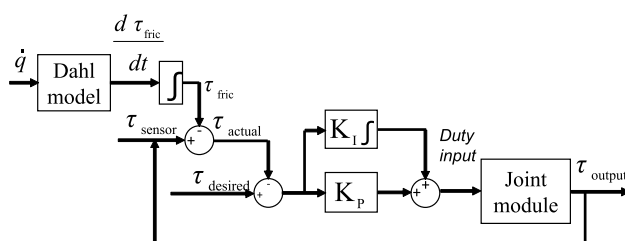


Fig. 9 Torque controller of the joint module with seal friction compensator

Table 3 Link length of the dual-arm UVMS

l_{w1}	l_{w2}	l_{w3}	l_{c1}	l_{c2}	l_{c3}
350 mm	250 mm	288 mm	382 mm	463 mm	423 mm

the encoder included in the joint modules. The configuration of the system was calculated from the joint angle data. The movement denoted on Fig. 11 shows the result of the first experiment with cooperation method. The desired trajectory of independent joints is the same for the both cases. Therefore, the trajectories with and without cooperation were almost the same; the difference could be caused by small torque and force errors during experiments.

Comparing each result with the simulation data, the trend in the experimental data is similar. Figure 13 shows a comparison of the manipulator torque between the simulation and experiment, and Fig. 14 shows the vehicle thrust force. The error between the simulation and experiment is mainly caused by nonlinear friction of the rotary seal. Because such friction is compensated using an open-loop compensator, the friction signal cannot be completely removed from the torque sensor data, which causes an error between the joint torque and the desired torque from the cooperative controller. In addition, slip between the end-effector of the working manipulator and the handle valve may cause a joint angle error, resulting in a difference between the simulation and experiment. To summarize the comparison, the experiments did not perfectly match the simulation, but the differences could be explained, and they showed similar tendencies.

By comparing two cases, one without cooperation and one with cooperation, the cooperation method showed a beneficial effect in reducing the burden of a dual-arm manipulator for the turning of the handle valve. Figure 15 shows a comparison of all data between both cases. On each data point, standard deviations were calculated from five experiments of each case. The 1σ error regions are denoted by the shaded area, and they confirm that the experiments were repeatable. The joint torques of all manipulators showed a

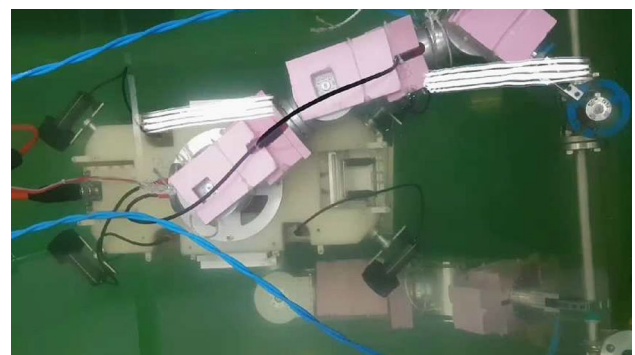


Fig. 10 Fabricated dual-arm UVMS and experiment setup

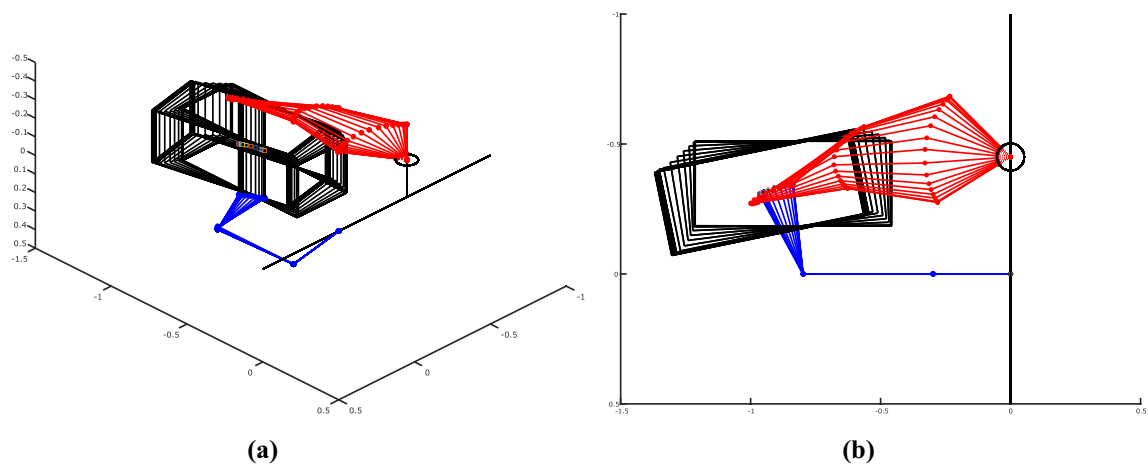
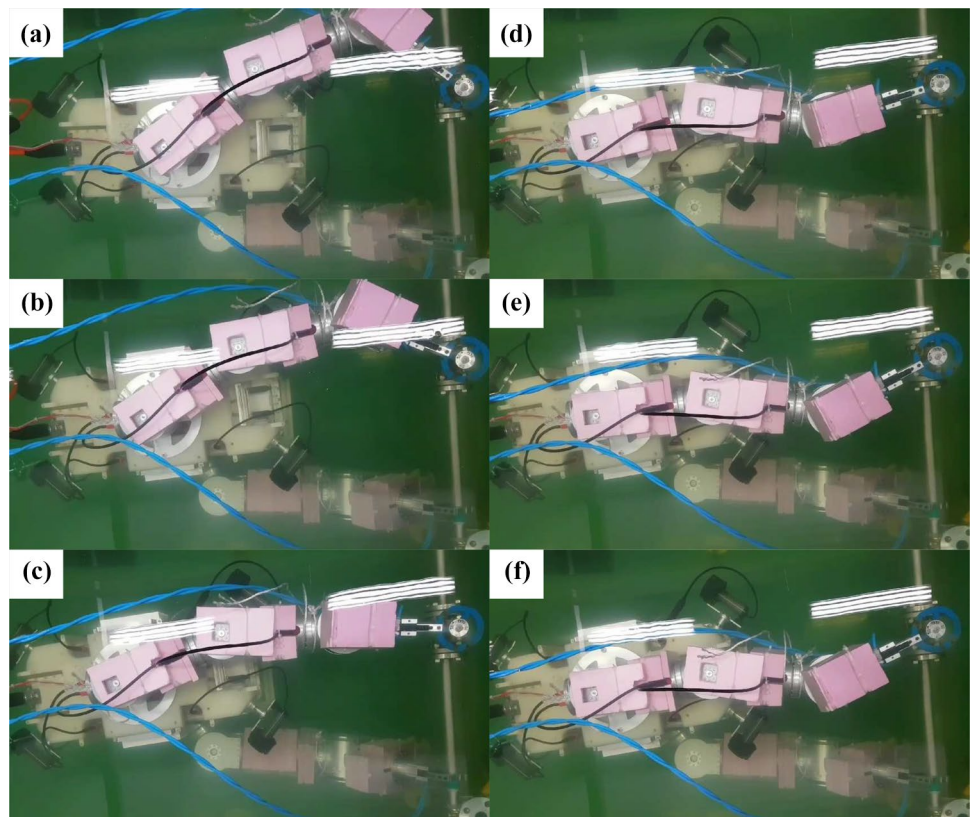


Fig. 11 The trajectory of the first experiment using cooperation method: **a** isometric view; **b** top view

Fig. 12 The snapshots of the valve turning experiments: **a** $t = 0$ s; **b** $t = 5$ s; **c** $t = 10$ s; **d** $t = 15$ s; **e** $t = 20$ s; **f** $t = 25$ s



tendency to be reduced when using the vehicle thrust force. The trajectory error of the handle valve was not changed when applying the cooperative controller, as shown in Figure 15 (b), which means the cooperation can be achieved without interfering with the main task, valve turning. The steady-state error of valve angle can be caused by joint angle or friction modeling error. We suspect joint angle errors are a major reason, because a small angle error can cause a large internal torque in closed-loop configuration.

Figure 16 summarizes the maximum torque of five joints of the manipulators during the operation. The maximum torque of joints W1, W2, and C1 shows little difference of no larger than 1σ error regions of the data. The torque of joints W3 and C2 was significantly reduced by over 30% of the maximum torque, which difference is much larger than 1σ error regions. Table 4 shows the effect of the cooperative manipulation method expressed as a percentage. By reducing the maximum joint torque using some of the

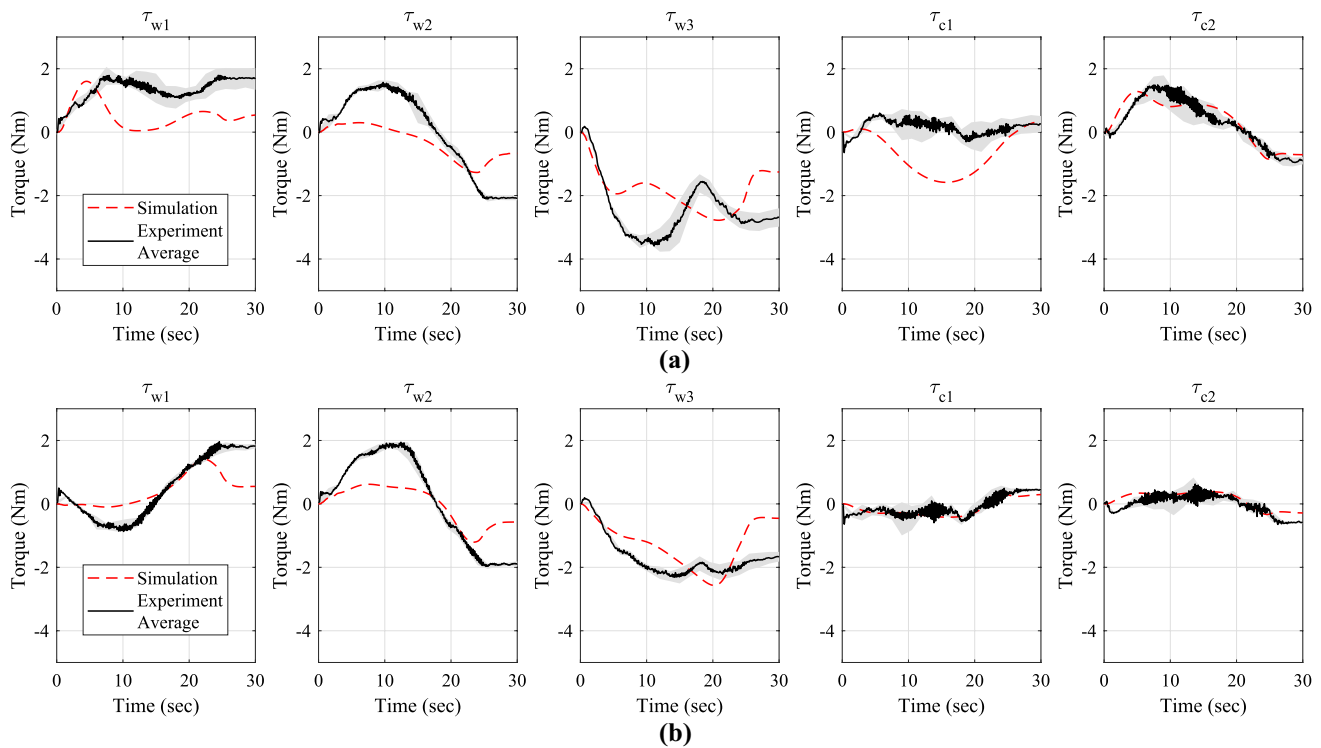


Fig. 13 Comparison of manipulator torque between simulation and experiment. The simulation data are denoted as a red dashed line, and the experiment data are denoted as a black line. The gray area denotes

the standard deviation of the experiments. Results **a** without and **b** with cooperation

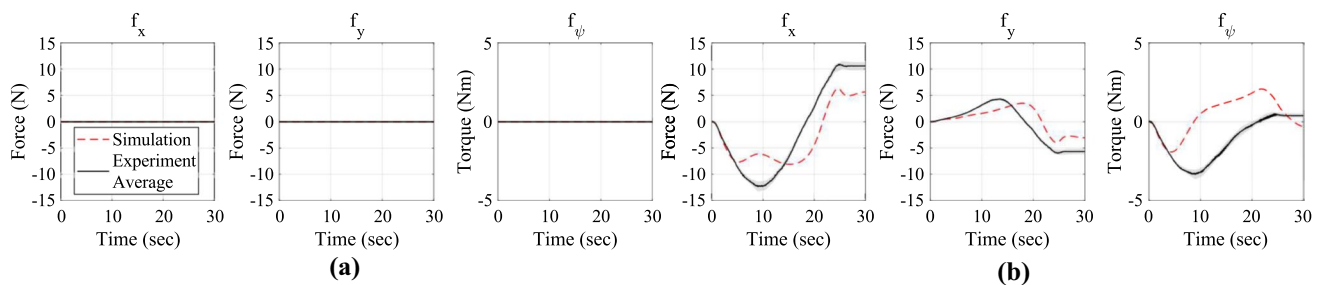


Fig. 14 Comparison of vehicle thrust force between simulation and experiment. The simulation data are denoted by the red dashed line, and the experiment data are denoted by the black line. The gray area denotes

the standard deviation of the experiments. Results **a** without and **b** with cooperation

vehicle thrust force, the task can be performed with a smaller manipulator, which is beneficial for the design of a mobile manipulator system.

5 Valve Turning Experimental Results under Disturbance

5.1 Disturbance Generation Device

The disturbance generator was designed and fabricated for conducting experiments under disturbance. Figure 17 shows the design and appearance of the generator. A spare thruster for the vehicle (BTD150, SEABOTIX, United States) was used to fabricate the generator. The generator

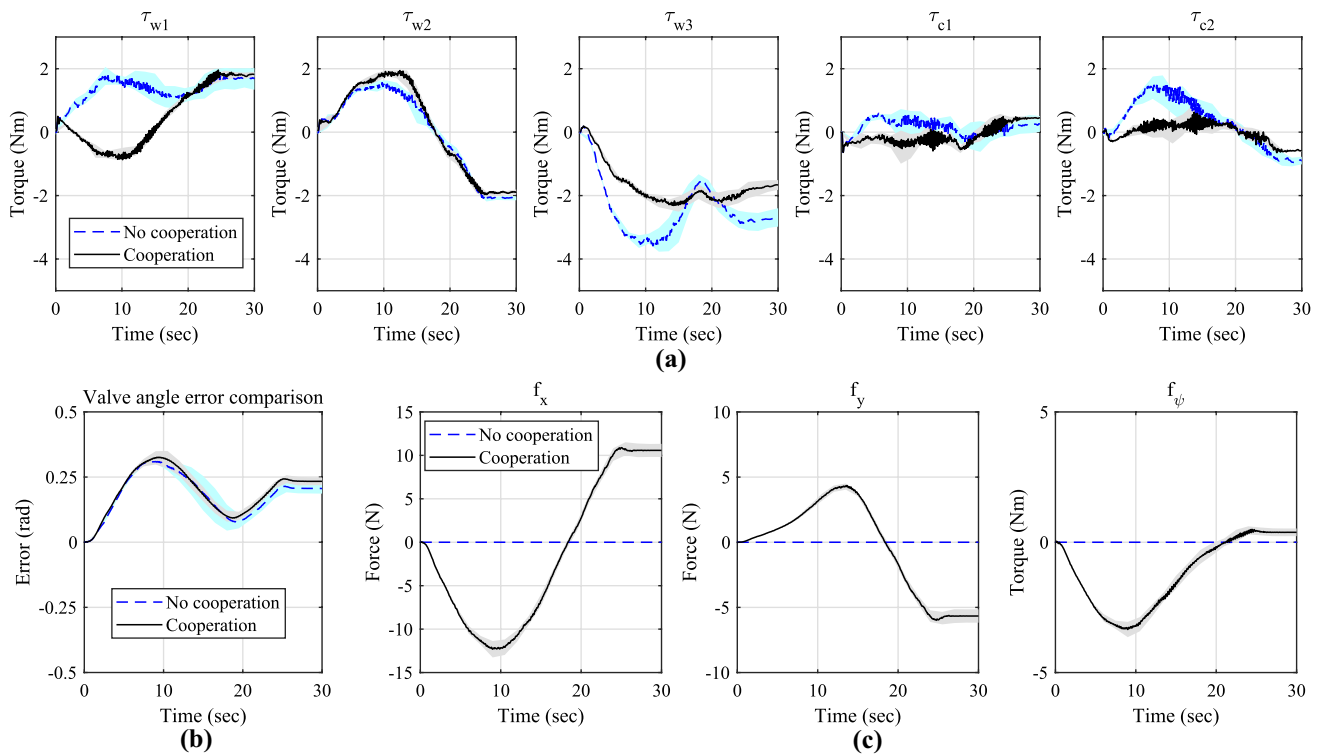


Fig. 15 Comparison of the joint torque of the manipulators and vehicle thrust force between the experiment without cooperation and the experiment with cooperation. The data without cooperation are denoted as the blue dashed line, and the data with cooperation are

denoted as the black line. The sky-blue and gray areas present the standard deviation of both types of data. **a** Joint torque of the manipulators, **b** trajectory error in the angle of the handle valve, and **c** vehicle thrust force

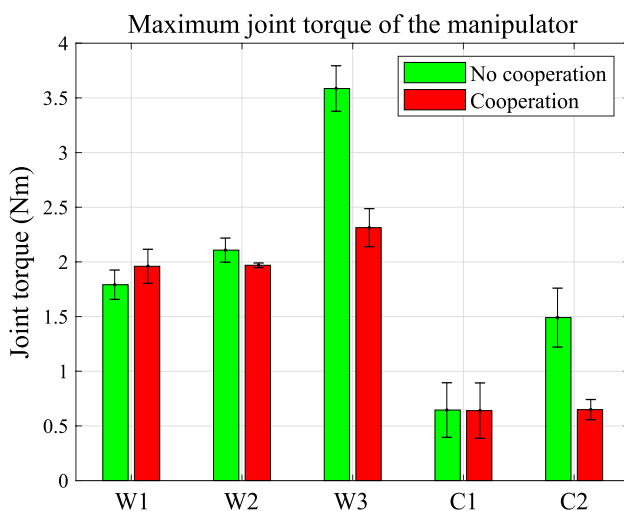


Fig. 16 Comparison of maximum torque of each manipulator joint. The error bar denotes the standard deviation of the maximum torque

Table 4 Effect of cooperation on maximum joint torque

Joints	W1	W2	W3	C1	C2
	↑ 10%	↓ 5%	↓ 36%	↓ 0.0%	↓ 60%

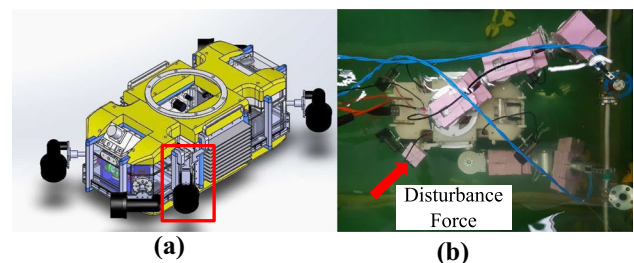


Fig. 17 Disturbance generator for compensation experiment. **a** Design of the generator and **b** disturbance generator attached to the UVMS

is attached to the vehicle and applies its thrust force to the vehicle, which can be assumed to be an external force from an oceanic current. Using a thruster as a disturbance generator makes it possible to control the size of disturbance force easily. The force was applied at 45° with respect to the vehicle direction, as shown in Fig. 17 (b). The size of the disturbance force can be adjusted using a pulse-width modulated signal input into the thruster driver.

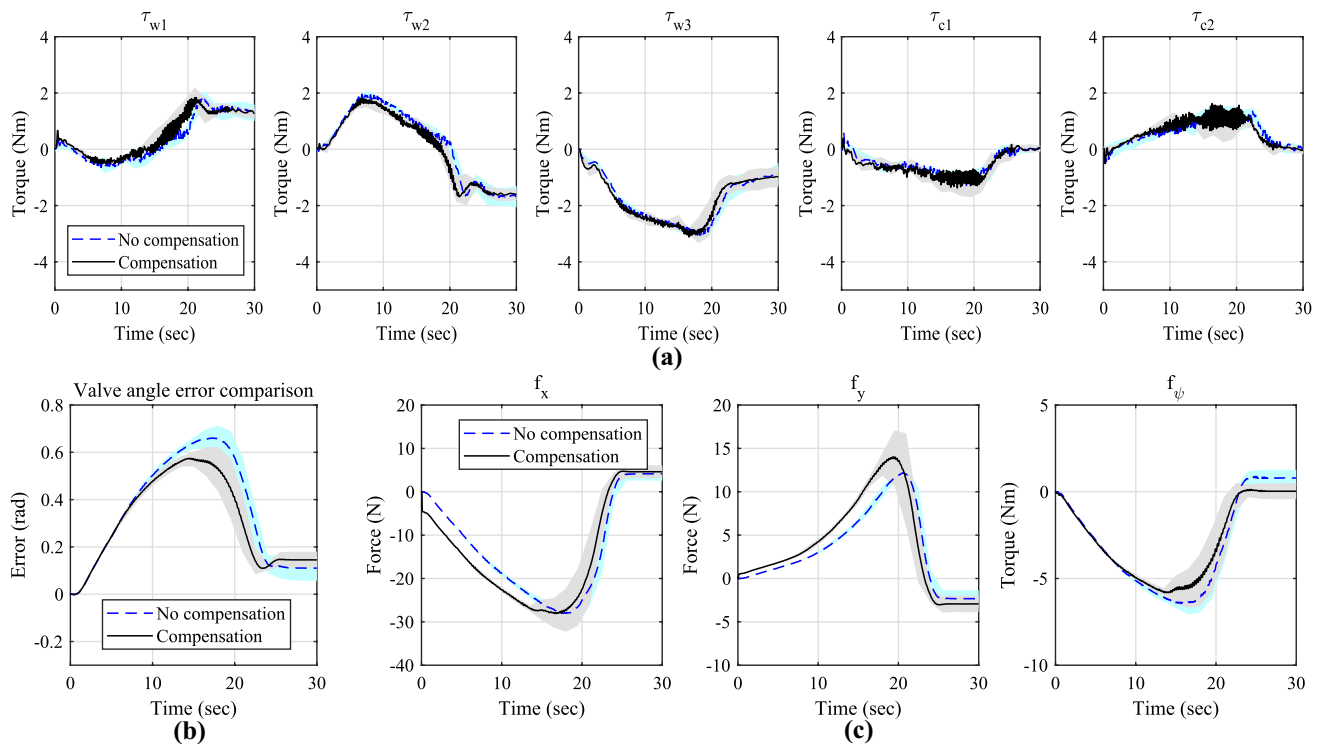


Fig. 18 Comparison of joint torque of the manipulators and vehicle thrust force under a disturbance between the experiment without a compensation term and the experiment with a compensation term. The data without a compensation are denoted with the blue dashed

line, and the data with a compensation are indicated using the black line. The sky-blue and gray areas present the standard deviation of two types of data. **a** Joint torque of the two manipulators, **b** trajectory error of the angle of the handle valve, and **c** the vehicle thrust force

cooperative manipulation method with a disturbance compensator, an external disturbance can be compensated during a valve turning operation without interfering with the main task. The trajectory error of the handle valve was reduced with a small amount of joint torque of the manipulators and the vehicle thrust force.

6 Conclusion

In this paper, a cooperative manipulation method including disturbance compensation was developed and proved experimentally. The objective task was set as the turning of a handle valve located underwater, which is an important task. A manipulation method for grasping a fixed structure during an operation was developed, and its kinematic and dynamic equations were derived. The concept of cooperation, in which the manipulators and the vehicle help each other, was developed by applying the kinematic properties of the system. The system has properties of a parallel manipulator; in addition, the force and torque can be distributed, and a large internal force can be generated with a small amount of torque. The cooperative manipulation method was formulated with modified redundancy resolution method of a parallel manipulator. The proposed cooperative

manipulation method was proved through a dynamic simulation and valve turning experiment. The experiments were conducted using a dual-arm UVMS, which was fabricated by connecting a dual-arm manipulator to and underwater vehicle. A waterproof electronic joint module was developed to fabricate the dual-arm manipulator. The simulation and experimental results indicate that by using the proposed cooperative method, the maximum torque of the manipulator was decreased when applying some of the vehicle thrust to the performance of the main task. In addition, the vehicle thrust force for compensating an external disturbance can be reduced using a small amount of joint torque of the manipulators. The proposed cooperative method is superior for reducing the manipulator size for the design of a mobile manipulator system. An additional disturbance observer will be developed for compensating external force from random ocean current.

Supplementary Information The online version contains supplementary material available at <https://doi.org/10.1007/s12541-022-00685-4>.

Acknowledgements This work was supported by the Basic Science Research Program and International Research Collaboration Program through the National Research Foundation (NRF) of Korea funded by the Ministry of Science, ICT (NRF-2017R1A2B4002123 and NRF-2017K1A3A1A19071037).

Declarations

Competing interest The authors declare that they have no conflict of interest.

References

- Ribas, D., Palomeras, N., Ridao, P., Carreras, M., & Mallios, A. (2012). Girona 500 auv: From survey to intervention. *IEEE/ASME Transactions on mechatronics*, 17(1), 46–53.
- Simetti, E., Casalino, G., Torelli, S., Sperinde, A., & Turetta, A. (2014). Floating underwater manipulation: Developed control methodology and experimental validation within the trident project. *Journal of Field Robotics*, 31(3), 364–385.
- Cieslak, P., Ridao, P., & Giergiel, M. (2015). Autonomous underwater panel operation by girona500 uvms: A practical approach to autonomous underwater manipulation. In: 2015 IEEE International Conference on robotics and automation (ICRA), pp. 529–536. IEEE.
- Ribas, D., Ridao, P., Turetta, A., Melchiorri, C., Palli, G., Fernández, J. J., & Sanz, P. J. (2015). I-auv mechatronics integration for the trident fp7 project. *IEEE/ASME Transactions on Mechatronics*, 20(5), 2583–2592.
- Khatib, O., Yeh, X., Brantner, G., Soe, B., Kim, B., Ganguly, S., et al. (2016). Ocean one: A robotic avatar for oceanic discovery. *IEEE Robotics & Automation Magazine*, 23(4), 20–29.
- Carrera, A., Ahmadzadeh, S., Ajoudani, A., Kormushev, P., Carreras, M., & Caldwell, D. G. (2012). Towards autonomous robotic valve turning. *Cybernetics and Information Technologies*, 12(3), 17–26.
- Youakim, D., Ridao, P., Palomeras, N., Spadafora, F., Ribas, D., & Muzzupappa, M. (2017). Moveit: Autonomous underwater free-floating manipulation. *IEEE Robotics & Automation Magazine*, 24(3), 41–51.
- Di Lillo, P., Simetti, E., Wanderlingh, F., Casalino, G., & Antonelli, G. (2020). Underwater intervention with remote supervision via satellite communication: Developed control architecture and experimental results within the dexrov project. *IEEE Transactions on Control Systems Technology*.
- Sivčev, S., Coleman, J., Omerdić, E., Dooly, G., & Toal, D. (2018). Underwater manipulators: A review. *Ocean Engineering*, 163, 431–450.
- Inoue, F., Muralami, T., & Ihnishi, K. (2001). A motion control of mobile manipulator with external force. *IEEE/ASME Transactions on Mechatronics*, 6(2), 137–142.
- Dietrich, A., Bussmann, K., Petit, F., Kotyczka, P., Ott, C., Lohmann, B., & Albu-Schäffer, A. (2016). Whole-body impedance control of wheeled mobile manipulators. *Autonomous Robots*, 40(3), 505–517.
- Han, J., Park, J., & Chung, W. K. (2011). Robust coordinated motion control of an underwater vehicle-manipulator system with minimizing restoring moments. *Ocean Engineering*, 38(10), 1197–1206.
- Ryll, M., Muscio, G., Pierri, F., Cataldi, E., Antonelli, G., Caccavale, F., et al. (2019). 6d interaction control with aerial robots: The flying end-effector paradigm. *The International Journal of Robotics Research*, 38(9), 1045–1062.
- Bae, J., Bak, J., Jin, S., Seo, T., & Kim, J. (2018). Optimal configuration and parametric design of an underwater vehicle manipulator system for a valve task. *Mechanism and Machine Theory*, 123, 76–88.
- Bae, J., Jin, S., Kim, J., & Seo, T. (2019). Comparative study on underwater manipulation methods for valve-turning operation. *Meccanica*, 54(6), 901–916.
- Taylor, A. J. (1993). Design issues for underwater manipulator systems. *Mechatronics*, 3(4), 419–432.
- Harada, K., Hirukawa, H., Kanehiro, F., Fujiwara, K., Kaneko, K., Kajita, S., & Nakamura, M. (2004). Dynamical balance of a humanoid robot grasping an environment. In: 2004 IEEE/RSJ International Conference on Intelligent Robots and Systems, vol. 2, pp. 1167–1173. IEEE.
- Koyanagi, K., Hirukawa, H., Hattori, S., Morisawa, M., Nakao, S., Harada, K., & Kajita, S. (2008). A pattern generator of humanoid robots walking on a rough terrain using a handrail. In: 2008 IEEE/RSJ International Conference on Intelligent Robots and Systems, pp. 2617–2622. IEEE.
- Lehmann, C., Olofsson, B., Nilsson, K., Halbauer, M., Haage, M., Robertsson, A., et al. (2013). Robot joint modeling and parameter identification using the clamping method. *IFAC Proceedings Volumes*, 46(9), 813–818.
- Seki, Y., Sagara, S., & Ambar, R. (2018). Impedance control of dual-arm 3-link underwater robot: In the case of grasping a fixed object lightly with one hand. In: 2018 International Conference on Information and Communication Technology Robotics (ICT-ROBOT), pp. 1–4. IEEE.
- Russakow, J., Khatib, O., & Rock, S.M. (1995). Extended operational space formulation for serial-to-parallel chain (branching) manipulators. In: Proceedings of 1995 IEEE International Conference on Robotics and Automation, vol. 1, pp. 1056–1061. IEEE.
- Casalino, G., & Turetta, A. (2003). Coordination and control of multiarm, non-holonomic mobile manipulators. In: Proceedings 2003 IEEE/RSJ International Conference on intelligent robots and systems, vol. 3, pp. 2203–2210. IEEE.
- Dietrich, A., Ott, C., & Albu-Schäffer, A. (2015). An overview of null space projections for redundant, torque-controlled robots. *The International Journal of Robotics Research*, 34(11), 1385–1400.
- Korpela, C., Orsag, M., & Oh, P. (2014). Towards valve turning using a dual-arm aerial manipulator. In: 2014 IEEE/RSJ International Conference on Intelligent Robots and Systems, pp. 3411–3416. IEEE.
- Cataldi, E., Real, F., Suárez, A., Di Lillo, P., Pierri, F., Antonelli, G., Caccavale, F., Heredia, G., & Ollero, A. (2019). Set-based inverse kinematics control of an anthropomorphic dual arm aerial manipulator. In: 2019 International Conference on robotics and automation (ICRA), pp. 2960–2966. IEEE.
- Moe, S., Antonelli, G., & Pettersen, K.Y. (2014). Null-space-based behavior guidance of planar dual-arm uvms. In: 2014 IEEE International Conference on Robotics and Biomimetics (ROBIO 2014), pp. 735–740. IEEE.
- Jin, S., Kim, J., Kim, J., & Seo, T. (2015). Six-degree-of-freedom hovering control of an underwater robotic platform with four tilting thrusters via selective switching control. *IEEE/ASME Transactions on Mechatronics*, 20(5), 2370–2378.
- Lee, S. (2008). (a) research on antagonistic stiffness for over-actuated parallel mechanisms. PhD thesis, Seoul National University.
- Spong, M.W., Hutchinson, S., & Vidyasagar, M., et al. (2006). Robot Modeling and Control.
- Schjølberg, I., & Fossen, T.I. (1994). Modelling and control of underwater vehicle-manipulator systems. In: in Proc. Rd Conf. on Marine Craft Maneuvering and Control. Citeseer.
- Cheng, H., Yiu, Y.-K., & Li, Z. (2003). Dynamics and control of redundantly actuated parallel manipulators. *IEEE/ASME Transactions on mechatronics*, 8(4), 483–491.
- Jin, S., Bae, J., Kim, J., & Seo, T. (2017). Disturbance compensation of a dual-arm underwater robot via redundant parallel mechanism theory. *Meccanica*, 52(7), 1711–1719.

33. Olsson, H., Åström, K. J., De Wit, C. C., Gäfvert, M., & Lischinsky, P. (1998). Friction models and friction compensation. *European Journal of Control*, 4(3), 176–195.

Publisher's Note Springer Nature remains neutral with regard to jurisdictional claims in published maps and institutional affiliations.



Jangho Bae received a BS degree in mechanical engineering and physics in Seoul National University, Republic of Korea in 2012. He received a PhD from the Department of Mechanical and Aerospace Engineering, Seoul National University, Republic of Korea in 2019. He is currently a postdoctoral researcher at GRASP Laboratory, University of Pennsylvania. His current research interests are mobile manipulation and dual-arm manipulation.



Yecheol Moon received his BS in 2018 from the School of Mechanical Engineering, Hanyang University and MS degree in 2020 from the Department of mechanical convergence engineering at Hanyang University, Seoul, Korea. He is currently a Ph. D. student at RoDEL, Hanyang University. His research interests include the design and control of robotic platforms and underwater robots.



Eugene Park was born in Seoul, Korea, in 1990. He received his BS and MS degrees in mechanical engineering from Seoul National University in 2017 and 2019, respectively. He is a robot engineer with extensive experience and knowledge. He has suggested and designed innovative ideas toward the optimized reconfiguration function of a variable topology truss platform developed through the Korea-US joint research project, Variable Truss for Robotic Humanitarian Missions 2017. He has also

designed joint modules used in underwater manipulators through cooperation between a vehicle and a robotic dual-arm with a clamp.



Jongwon Kim received a BS degree in mechanical engineering from Seoul National University, Korea in 1978, an MS degree in mechanical and aerospace engineering from the Korea Advanced Institute of Science and Technology, Korea in 1980, and a PhD in mechanical engineering from the University of Wisconsin-Madison, USA in 1987. He is an honorary professor at the School of Mechanical and Aerospace Engineering, Seoul National University, Korea. His current research

interests include parallel mechanisms, Taguchi methodology, and field robots.



Sangrok Jin received a BS degree in 2008 and a PhD in 2014 from the School of Mechanical and Aerospace Engineering, Seoul National University, Seoul, South Korea. He was a post-doctoral researcher at Seoul National University from 2014 to 2016. From 2016 to 2017, he was a senior research associate with the University of Texas Health Science Center, Houston, TX, USA. Since 2017, he has been an assistant professor with Pusan National University, Pusan, South Korea. His

research interests include the design and control of robotic systems.



TaeWon Seo received a BS degree and PhD from the School of Mechanical and Aerospace Engineering, Seoul National University. He is a professor at the School of Mechanical Engineering, Hanyang University. Before that, he was a postdoctoral researcher at Nanorobotics Laboratories, Carnegie Mellon University, a visiting professor at Biomimetic Millisystems Laboratories, UC Berkeley, and an associate and assistant professor at the School of Mechanical Engineering, Yeungnam University, Korea. His research interests include robot design, analysis, control, optimization, and planning. Dr. Seo received the Best Paper Award of the IEEE/ASME Transaction on Mechatronics in 2014, and is currently working as a technical editor of IEEE/ASME Transaction on Mechatronics, and as an associate editor of IEEE Robotics and Automation Letters, and Intelligent Service Robots.

His research interests include robot design, analysis, control, optimization, and planning. Dr. Seo received the Best Paper Award of the IEEE/ASME Transaction on Mechatronics in 2014, and is currently working as a technical editor of IEEE/ASME Transaction on Mechatronics, and as an associate editor of IEEE Robotics and Automation Letters, and Intelligent Service Robots.